HHS Public Access

Author manuscript

*Cell Chem Biol*. Author manuscript; available in PMC 2024 September 21.

Published in final edited form as:

*Cell Chem Biol*. 2023 September 21; 30(9): 1053–1063.e5. doi:10.1016/j.chembiol.2023.07.003.

# Genetic activation of glycolysis in osteoblasts preserves bone mass in type I diabetes

**Xing Ji**[1], **Rebecca Seeley**[1], **Ke Li**[1], **Fangfang Song**[1], **Xueyang Liao**[1], **Chao Song**[1], **Marco Angelozzi**[1], **Arianna Valeri**[1], **Tyler Marmo**[1], **Wen-Chih Lee**[1], **Yu Shi**[1], **Fanxin Long**[1,2,*]

[1]Translational Research Program in Pediatric Orthopedics, Department of Surgery, The Children's Hospital of Philadelphia, Philadelphia, PA

[2]Deaprtment of Orthopedic Surgery, University of Pennsylvania, Philadelphia, PA

## Summary

Type I diabetes (T1D) impairs bone accrual in patients, but the mechanism is unclear. Here in a murine monogenic model for T1D, we demonstrate that diabetes suppresses bone formation resulting in a rapid loss of both cortical and trabecular bone. Single-cell RNA sequencing uncovers metabolic dysregulation in bone marrow osteogenic cells of the diabetic mice. In vivo stable isotope tracing reveals impaired glycolysis in diabetic bone that is highly responsive to insulin stimulation. Remarkably, deletion of the insulin receptor reduces cortical but not trabecular bone. Increasing glucose uptake by overexpressing Glut1 in osteoblasts exacerbates bone defects in T1D mice. Conversely, activation of glycolysis by Pfkfb3 overexpression preserves both trabecular and cortical bone mass in the face of diabetes. The study identifies defective glucose metabolism in osteoblasts as a pathogenic mechanism for osteopenia in T1D, and furthermore implicates boosting osteoblast glycolysis as a potential bone anabolic therapy.

## Graphical Abstract

[*]Lead contact, Corresponding author: Fanxin Long, longf1@chop.edu.

Author contributions

XJ performed experiments, analyzed data, prepared figures and wrote methods. RS, KL, FS, XL, CS, YS, WL, AV, TM helped with experiments. MA assisted with scRNA-seq data analysis. FL directed the project and wrote the paper.



Declaration of Interests

The authors declare no competing interests.

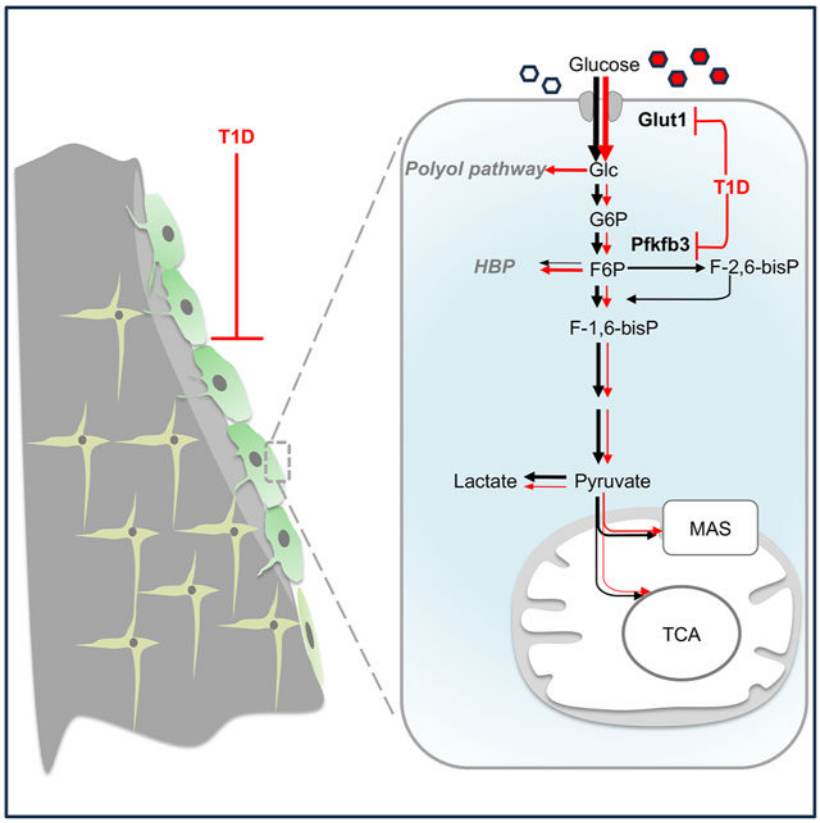


## eTOC Blurb

Ji et al demonstrate that impaired glycolysis in osteoblasts, the chief bone-making cells, is responsible for bone loss in a monogenic type I diabetes mouse model. They further provide a proof of principle that targeted activation of glycolysis in osteoblasts can be exploited for a bone therapy in diabetes.

## Introduction

Mounting evidence indicates that diabetes is associated with increased bone fracture risks [1-4]. As most studies show that both bone formation and resorption are suppressed in diabetic patients, bone anabolic therapies are likely needed for effective treatment of diabetic bone frailty [5]. The current options, however, are limited, as romosozumab carries potential risks of cardiovascular diseases, whereas teriparatide or abaloparatide cannot be used in children due to concerns about osteosarcoma [6-8]. Therefore, there remains an unmet need for safe anabolic therapies to combat diabetic bone frailty especially in children.

The cellular and molecular mechanisms underlying diabetic bone fragility are not well understood and likely multifaceted [9]. Both loss of insulin and hyperglycemia could potentially contribute to bone defects in type I diabetes (T1D). Genetic deletion of the insulin receptor (IR) in mature osteoblasts has been shown to suppress both bone formation and resorption in the mouse, resulting in a net loss of trabecular but not cortical bone mass [10,11]. However, it is not known whether loss of insulin signaling at an earlier stage

of the osteoblast lineage would similarly affect bone accrual. Moreover, a genetically reconstituted IR knockout mice that maintained euglycemia did not exhibit a bone defect despite no IR was expressed in bone, thus raising questions about a direct role for insulin signaling in osteoblasts, even though potential compensation from Igf1r upregulation could not be ruled out in that study[12]. Studies of hyperglycemia have been most active around advanced glycation end products (AGE) that not only impair the physical properties of bone matrix but could also potentially affect bone mass through RAGE signaling [13]. However, it is not known how chronic hyperglycemia might diminish osteoblast differentiation or activity. Overall, both the extent and the mechanism for hypoinsulinemia or hyperglycemia to influence diabetic osteopenia remain to be elucidated.

Recent studies have demonstrated that bone anabolic signals including Wnt, PTH and Igf promote bone formation partly through stimulation of glucose, fatty acid or glutamine metabolism [14-17]. Conversely, Notch signaling suppresses osteoblast differentiation through inhibition of glucose metabolism in mesenchymal progenitors [18]. Such findings demonstrate that osteoblast metabolism is highly attuned to bone anabolic needs in response to paracrine and endocrine signals. Potential metabolic changes in osteoblasts could contribute to diabetic osteopenia but have not been demonstrated to date.

Akita mice harbor a single nucleotide mutation in the Ins2 gene that disrupts the formation of a disulfide bond between the A and B chains of insulin 2, resulting in misfolding of the hormone and endoplasmic reticulum (ER) stress-mediated toxicity in pancreatic ß cells [19-21]. The heterozygous male Akita mice in the C57BL6 background develop clear diabetes by 3-4 weeks but can live for over 300 days, and offer an advantageous choice for studying the effects of hypoinsulinemia and hyperglycemia with fewer confounding effects than other T1D models such as that induced by streptozotocin [22]. Previous studies have reported bone loss in the Akita diabetic mice, but the pathophysiological mechanisms are yet to be elucidated [22,23].

Here we show that impaired osteoblast differentiation and bone formation drives diabetic osteopenia in the Akita mice. In vivo glucose tracing and scRNA-seq reveal cell intrinsic metabolic defects in osteoblast-lineage cells in response to diabetes. Loss of direct insulin signaling diminishes cortical bone growth whereas hyperglycemia is likely responsible for trabecular bone loss in T1D. Importantly, cell-autonomous activation of glycolysis in osteoblasts increases bone mass in the diabetic mouse. Thus, boosting glycolysis in osteoblasts may be a viable strategy for countering bone loss in diabetes.

## Results

### T1D causes rapid onset of osteopenia via suppression of bone formation

To begin the studies of diabetic osteopenia, we have monitored the bone phenotype along with diabetes progression in Akita mice. As expected, the heterozygous males developed notable hyperglycemia (fasting glucose level >300 mg/dL) due to a marked decrease in the circulating insulin beginning at 4 weeks of age (Fig. 1A, B). The circulating insulin-related growth factor 1 was also slightly reduced in 8-week-old Akita mice (Supplemental Figure S1A). Bone imaging and quantification by μCT detected a clear deficit in both cortical and

trabecular bone in Akita mice soon after the onset of diabetes. In particular, the cortical bone area was reduced at 4 weeks whereas the total area and cortical thickness of the bone shaft was also decreased at 8 weeks (Fig. 1C-E, S1B). The trabecular bone was diminished by 8 weeks, mainly due to reduced trabecular thickness causing a lower trabecular bone volume (Fig. 1F, S1C-G). The bone loss was independent of body weight which was normal in the Akita mice until at least 8 weeks of age (Fig. S1H). Serum biochemical assays showed that the level of P1NP, a marker for bone formation, was significantly lower in Akita at 8 and 20 weeks of age (Fig. 1G). The bone resorption maker CTX-I, on the other hand, exhibited a downward trend at all time points without reaching statistical significance (Fig. 1H). Nonetheless, histomorphometry with TRAP staining demonstrated a reduced osteoclast number in Akita at 8 weeks of age (Fig. 1I, J). Dynamic histomorphometry revealed significant decreases in mineralizing surface (MS/BS) and bone formation rate (BFR) in both trabecular bone and the periosteum of 8-week-old Akita (Fig. 1K, L, Supplemental S1I, J). Thus, T1D in the Akita mice acutely suppresses both trabecular and cortical bone accrual through inhibition of bone formation.

## T1D impairs metabolism and differentiation of osteoblast lineage cells

To gain insights about the osteogenic defect at the single cell and transcriptomic level, we conducted scRNA-seq with bone marrow mesenchymal cells isolated from the metaphysis and endosteum of long bones (hereafter endosteal cells) in diabetic versus normal mice. The endosteal cells were purified by negative selection against the hematopoietic cells with FACS before they were subjected to scRNA-seq with the 10x genomics platform. Both 8- and 20-week-old mice were studied to reflect the disease progression. The initial analyses identified a total of 19 cell clusters all shared between control and Akita mice at both ages (Supplemental Fig. S2A, C). Most of the cells were mesenchymal cells expressing Prrx1 and Runx2, among smaller populations of smooth muscle cells, endothelial cells, platelet, red blood cells and other hematopoietic cells (Supplemental Fig. S2B, D). Secondary clustering of the mesenchymal cells identified 8 or 7 clusters in 8- or 20-week-old mice, respectively (Fig. 2A, Supplemental Fig. S3A). At both ages, a large majority (70-90%) of the mesenchymal cells expressed high levels of Cxcl12, Lepr, Adipoq, Lpl, Apoe and Ebf3, and were likely Adipo-CAR (Cxcl12 abundant reticular) cells as previously described [24] (Fig. 2A, B, Supplemental Fig. S3A, B). One cluster (#2 at 8 wks and #4 at 20 wks) expressed a lower level of the CAR cell markers but also the osteoblast markers Sp7, Bglap2, Alpl and Clec11a, and was designated Osteo-CAR cells [24]. The remaining cells (clusters 3, 8 at 8 wks; clusters 6 at 20 wks) are osteoblasts expressing various levels of Sp7, Bglap2, Alpl, Clec11a, Ifitm5, Dmp1, and Me2 which was recently shown to upregulate with osteoblast differentiation [25] (Fig. 2A, B, Supplemental Fig. S3A, B). At 8 weeks, diabetes reduced the relative abundance of Osteo-CAR and osteoblasts from 12.7% to 9.8% and from 13.6% to 9.1%, respectively, with a reciprocal increase of Adipo-CAR from 73.7% to 81.2%. The decrease in Osteo-CAR and osteoblasts versus increase in Adipo-CAR was also observed at 20 weeks (Supplemental Fig. S3A). Thus, T1D modestly reduces the osteogenic population among the bone marrow mesenchymal cells.

Diabetes could disrupt normal biological activities in the osteogenic cell types. To uncover such potential changes, we performed Gene Set Enrichment Analysis (GSEA) with the

scRNA-seq data to compare gene expression in osteogenic clusters from Akita versus normal mice. Notably, both glycolysis and oxidative phosphorylation (OXPHOS), along with mTORC1 signaling, were downregulated in Osteo-CAR cluster 2 and osteoblast cluster 3 of the Akita mice at 8 weeks of age, indicating impaired bioenergetic and biosynthetic activities (Fig. 2C, D, Supplemental Table I, II). Similarly, OXPHOS was reduced in osteoblast cluster 8 (Fig. 2E, Supplemental Table III). Interestingly, at 20 weeks, the metabolic changes were reversed, with OXPHOS and the related pathways including reactive oxygen species and fatty acid metabolism increased in the osteoblast cluster of Akita (Supplemental Fig. S3C, Supplemental Table IV). Similarly, Myc targets were upregulated in both Osteo-CAR and osteoblast of Akita at 20 weeks, in contrast to 8 weeks when they were markedly suppressed (Supplemental Fig. S3C, D, Supplemental Table V). Thus, T1D suppresses bioenergetic and anabolic pathways in bone marrow osteogenic cells initially but appears to cause maladaptive gene upregulation following progression of the disease.

To verify the metabolic changes detected by scRNA-seq, we measured the extracellular flux in primary cultures of endosteal cells with a Seahorse analyzer. Like for scRNA-seq, endosteal cells were isolated from the metaphysis and the endosteum of bone draft. They were cultured and then purified by immune depletion of $CD45^+$ hematopoietic cells with magnetic beads before the assays. The cells from 8-week-old Akita exhibited marked deficiency in both oxygen consumption rate (OCR) and extracellular acidification rate (ECAR) (Fig. 2F, G). The data therefore confirm that T1D at least during the early phase of the disease reduces both glycolysis and OXPHOS in bone marrow osteogenic cells.

The reduced abundance of osteogenic cells according to scRNA-seq indicates that osteoblast differentiation may be defective in the diabetic Akita mice. To test this possibility directly, we performed in vitro osteoblast differentiation with bone marrow stromal cells (BMSC) from 8-week-old Akita versus control mice. BMSC were flushed from the central marrow and purified through immune depletion of $CD45^+$ hematopoietic cells before being cultured in mineralization media for differentiation. Quantification of molecular markers confirmed that osteoblast differentiation was impaired in BMSC from the Akita mice (Fig. 2H). Thus, data from both scRNA-seq and in vitro studies provide evidence that T1D impairs both cell metabolism and osteogenic differentiation in osteoblast-lineage cells.

## T1D diminishes glycolysis in intact bone

To confirm the metabolic defect in bone cells in vivo, we performed glucose tracing experiments to determine the enrichment of labeled metabolites derived from labeled glucose via either glycolysis or the tricarboxylic acid (TCA) cycle (Fig. 3A). To this end, glucose uniformly labeled with stable isotope $^{13}C$ ($^{13}C_6$-Glc) was injected into 20-week-old mice, followed by extraction of the bone metabolites and quantification with mass spectrometry (Fig. 3B). To test the effect of insulin, the hormone was either co-injected with glucose for the wild type mice, or injected one hour prior to glucose for the Akita mice (Fig. 3B). The different insulin regimen was chosen purposefully to ensure the blood glucose level to be within the normal range at time of harvest for both genotypes (Fig. 3C). The enrichment of (m+6)Glc in both plasma and bone, as indicated by atom percentage

excess (APE), was lower in Akita, whereas insulin reduced (m+6)Glc enrichment in both wild type and Akita mice, with a greater effect on bone than plasma (Supplemental Fig. S4A, D). Similarly, (m+3)Lac in both plasma and bone was lower in Akita, but it was increased by insulin, more so in bone than plasma (Supplemental Fig. S4B, E). The increase of (m+3)Lac by insulin was not seen in wild type mice which either showed no effect in bone or a decrease in plasma (Supplemental Fig. S4B, E). Importantly, when (m+3)Lac APE was normalized to (m+6)Glc APE to approximate the glycolytic flux, the ratio in bone was significantly lower in Akita. Moreover, insulin increased that ratio in both wild type and Akita bones, with a greater effect on Akita (Fig. 3D). In the blood, insulin increased the ratio only in Akita but not wild type (Supplemental Fig. S4C). Except for malate, little labeling of the TCA metabolites was detected in bone, confirming lactic acid as the predominant fate for glucose in osteoblasts and osteocytes. The labeled malate in wild type bone was in the form of (m+3) instead of (m+2), consistent with our previous finding in osteoblast cultures [25] (Supplemental Fig. S4F, G). The labeled malate was undetectable in Akita bone, indicating likely disruption of the malate-aspartate shuttle important for sustaining glycolysis in osteoblasts (Supplemental Fig. S4F) [25]. Insulin increased (m+3)Mal in wild type or Akita bone, both before and after normalization to (m+6)Glc (Fig. 3E, Supplemental Fig. S4F). Intriguingly, insulin increased (m+2)Mal only in wild type bone, indicating that insulin normally stimulates glucose oxidation in the TCA cycle but the response is impaired in the diabetic bone (Fig. 3F, Supplemental Fig. S4G). Overall, the metabolic flux studies show that T1D suppresses glycolysis in bone and that insulin stimulates bone glycolysis in both normal and T1D mice.

To examine potential metabolic changes at an earlier stage of T1D, we performed glucose tracing experiments in 8-week-old mice. The bone (m+3)Lac/(m+6)Glc ratio was normal in the Akita mice at this age (Fig. 3G). However, the flux analyses following the relatively short 1 hr labeling period might miss certain changes below the detection threshold. We therefore proceeded to measure the overall pool sizes of selective metabolites (labeled plus unlabeled) in bone. We focused on pyruvate which is the end product of the core glycolysis pathway, and the potential downstream metabolites. The amount of lactate relative to pyruvate was significantly diminished in Akita, whereas the TCA cycle metabolites including citrate, succinate and fumarate were not affected (Fig. 3H-K). Thus, the metabolic fate of pyruvate towards lactate appeared to be selectively suppressed in the Akita bone. To ascertain that the metabolic defect observed in the bone tissue reflected impairments in osteoblast-lineage cells, we cultured the cells from cortical bone chips prepared from the long bones of 8-week-old wild-type versus Akita mice. The cells were depleted of hematopoietic cells with CD45-antibody-coated magnetic beads before use. Both glucose consumption and lactate production were significantly reduced in the bone-chip cells from Akita (Fig. 3L, M). Overall, the data from 8 and 20 weeks of age together support that T1D progressively suppresses glycolysis in bone cells.

## Both insulin and hyperglycemia affect osteoblast metabolism

To directly examine the metabolic effect of insulin on osteoblast-lineage cells, we set out to measure the extracellular flux in primary cell cultures with Seahorse technology. Bone-chip cells, central marrow BMSC, periosteal cells as well as endosteal cells were cultured from

wild type mice and purified by immuno-depletion of hematopoietic cells. The cells were treated with insulin at physiological levels for 1 hr before the measurements. In bone-chip cells, insulin at either 1 or 10 ng/ml similarly boosted OCR including both ATP-producing and spare OCR, whereas 10 ng/ml also increased ECAR (Fig. 4A, B). Similarly, in BMSC or periosteal cells insulin at either concentration stimulated both OCR and ECAR (Fig. 4C, D, Supplemental Fig. S5A, B). On the other hand, endosteal cells did not respond to insulin in either OCR or ECAR (Supplemental Fig. S5C, D). Thus, insulin stimulates glucose metabolism in most if not all cells of the osteoblast lineage.

We next determined whether chronic hyperglycemia associated with diabetes could directly impact metabolism in osteoblast-lineage cells. For this, the cells were cultured with either 5.5 or 25 mM glucose for 14 days before being measured in normal Seahorse assay media. High glucose significantly reduced ECAR without an obvious effect on OCR in bone-chip cells (Fig. 4E, F). High glucose appeared to suppress both OCR and ECAR in endosteal cells, even though only ECAR reached statistical significance likely due to the small sample size (Supplemental Fig. S5E, F). Thus, chronic hyperglycemia suppresses glycolysis in osteoblast-lineage cells.

## Loss of insulin signaling impairs cortical but not trabecular bone accrual

To assess the contribution of defective insulin signaling to bone loss in T1D, we generated mice with the insulin receptor IR deleted in all limb connective tissues including bone, by using Prx1Cre. The males were analyzed at 8 and 20 wks of age to be consistent with the Akita mice. The IR conditional knockout mice (CKO) had normal body weight and length, normal bone length as well as normal circulating glucose levels (Supplemental Fig. S6A). However, μCT analyses of the femur showed that CKO, like Akita, exhibited a notable decrease in cortical bone area, cortical total area and cortical thickness, at both 8 and 20 wks of age (Fig. 5A, B). In contrast, no changes were detected in any of the trabecular bone parameters at either age (Fig. 5C, Supplemental Fig. S6B). Dynamic histomorphometry demonstrated a significant reduction in bone formation at the periosteal surface but not in trabecular bone or at the endosteum (Fig. 5D-F). Thus, direct loss of insulin signaling in the skeletal tissue restricts cortical bone accrual but cannot account for trabecular bone loss in T1D.

## Overexpression of Glut1 exacerbates osteopenia in T1D

We next investigated the biochemical basis for impaired glycolysis in the diabetic bone. Western blots showed that the glucose transporter Glut1 was already reduced in Akita at 8 weeks of age and further decreased by 20 weeks (Fig. 6A, B). Pfkfb3, a key enzyme producing a potent allosteric activator of glycolysis, was not significantly altered at 8 weeks but reduced by >50% at 20 weeks. Next-generation sequencing of cortical bone RNA revealed that Slc2a1, encoding Glut1, was notably reduced in Akita at 20 weeks of age (Fig. 6C). In contrast, several other genes related to carbon metabolism, including Fbp2 which promotes gluconeogenesis, Aldob known to favor fructose metabolism, and Pdk4 that reduces glucose oxidation in mitochondria, were all upregulated in Akita. Moreover, Txnip, well documented to suppress glycolysis, was significantly elevated in the Akita bone (Fig.

6C). Thus, T1D disrupts glycolysis in bone through dysregulation of glucose metabolism genes at both protein and mRNA levels.

The early decrease of Glut1 protein in the diabetic bone could be a cause for reduced glycolysis or a protective mechanism in response to systemic hyperglycemia. To distinguish these possibilities, we force-expressed Glut1 in osteoblasts of Akita mice to assess the potential effect on the diabetic bone phenotype. To this end, mice with either *Osx-rtTA;TRE-Glut1;Akita* (triple transgenic) or the control genotypes were fed food containing doxycycline (Dox) starting at 3 weeks of age. Dox increased Glut1 protein similarly in the bones of either *Osx-rtTA;TRE-Glut1* or triple transgenic mice compared to wild type or Akita mice when harvested at 8 weeks of age (Fig. 6D). Quantification with μCT showed that Glut1 overexpression in the normal background did not alter cortical or trabecular bone mass at either 8 or 20 weeks of age, even though it slightly increased trabecular number and reduced trabecular spacing at 8 weeks (Fig. 6E, F, Supplemental Fig. S6C-H). Importantly, the triple transgenic mice exhibited a further decease in cortical total area, cortical bone area and cortical thickness compared to Akita at 8 weeks (Fig. 6E, Supplemental Fig. S6C). The cortical total area remained smaller in the triple transgenic mice than Akita at 20 weeks of age (Fig. 6E). The trabecular bone fraction (BV/TV) showed a downward trend without reaching statistical significance in the triple transgenics compared to Akita at 8 weeks (Fig. 6F). However, the trabecular tissue volume (Tb. TV) and trabecular number (Tb. N) were further reduced with a corresponding increase in trabecular spacing (Tb. Sp) in the 8-week-old triple transgenic mice (Supplemental Fig. S6E, F, H). Serum biochemical assays revealed that Glut1 overexpression suppressed the bone formation marker P1NP in Akita (two-way ANOVA interaction $p < 0.05$) without affecting the bone resorption marker CTX-I (Fig. 6G, Supplemental Fig. S6I). Finally, overexpression of Glut1 in bone did not modify the high glucose level in the circulation of Akita mice (Supplemental Fig. S6J). Overall, forced expression of Glut1 in osteoblasts further impairs bone formation in the diabetic mouse. The finding therefore supports Glut1 downregulation as a protective mechanism for osteoblasts to mitigate excessive glucose uptake in diabetes.

## Overexpression of Pfkfb3 preserves bone mass in T1D

We next sought to uncover key glycolysis enzymes that can be targeted for activation of the pathway. The dCas9-SAM method was used in primary calvarial cell cultures to activate gene expression from the endogenous locus by targeting the promoter region with gene-specific sgRNA. Compared to Hk2 or Ldha, targeted activation of Pfkfb3 by one of the three guide RNAs tested uniquely increased glucose consumption and lactate production in primary calvarial preosteoblasts (Supplemental Fig. S7A-D). We therefore proceeded to create a mouse strain that can be induced to overexpress Pfkfb3 in response to Dox; the allele is termed R26-TRE-Pfkfb3 (TRE-Pfkfb3 for short hereafter) (Supplemental Fig. S7E). To validate the new mouse line, we crossed it with *Osx-rtTA* mice to generate progenies with the genotype of *Osx-rtTA;TRE-Pfkfb3* or *Osx-rtTA*, and then subjected both genotypes to Dox food from 3 through 8 weeks of age before harvest. Western blots of the bone protein extracts revealed notable upregulation of Glut1, Hk2 and Ldha, along with the expected induction of Pfkfb3 (Fig. 7A). The concurrent upregulation of the key glycolysis proteins provided evidence that Pfkfb3 overexpression activated the glycolysis pathway in

osteoblasts in vivo. We then bred the *Osx-rtTA;TRE-Pfkfb3* mice with the Akita strain to induce Pfkfb3 overexpression in the diabetic background. As predicted, Dox treatment of the male progenies from 3 through 8 weeks of age increased Pfkfb3 in the bones of either *Osx-rtTA;TRE-Pfkfb3* or *Osx-rtTA;TRE-Pfkfb3;Akita* mice (Fig. 7B). μCT analyses showed that Pfkfb3 overexpression in the wild-type background had no effect on most bone parameters at either 8 or 20 weeks of age, except for an increase in trabecular tissue volume at 20 weeks of age (Fig. 7C-H, Supplemental Fig. S7F-J). Nonetheless, essentially all parameters of trabecular or cortical bone were fully rescued in the triple transgenic mice (*Osx-rtTA;TRE-Pfkfb3;Akita*) compared to Akita (*TRE-Pfkfb3;Akita*) at 8 weeks of age (Fig. 7C-H, Supplemental Fig. S7F-J). At 20 weeks, the rescue of trabecular bone parameters became less obvious, but cortical bone thickness and area remained significantly improved in triple transgenics over Akita (Fig. 7D, G, H). Thus, forced expression of Pfkfb3 in osteoblasts effectively alleviates bone loss especially during the early phase of T1D.

We next examined the cellular effect of Pfkfb3 overexpression in osteoblasts. The serum P1NP level in triple transgenic mice was restored to the wild-type level at 8 weeks, and trended higher than Akita without reaching statistical significance at 20 weeks (Fig. 7I). Serum CTX-I levels on the other hand were similar across all genotypes at either age (Fig. 7J). Dynamic histomorphometry revealed that Pfkfb3 overexpression in Akita significantly increased osteoblast activity (MAR) resulting in increased bone formation rate (BFR) in both trabecular bone and at the endosteum (Fig. 7K, L). Despite the improved bone phenotype, Pfkfb3 overexpression did not alleviate the diabetic phenotype as neither body weight nor fasting glucose levels were different between the triple transgenics and Akita at either 8 or 20 weeks of age (Supplemental Fig. S7K, L). Taken together, the results show that cell-autonomous activation of glycolysis in osteoblasts protects against diabetic osteopenia in T1D by preserving bone formation activity.

## Discussion

The study systematically investigates the cellular and molecular mechanism responsible for osteopenia in a T1D mouse model. The results identify osteoblast dysfunction due to impaired glucose metabolism as an underlying cause for bone loss in the diabetic mice. Loss of insulin signaling can account for the cortical bone defect, but hyperglycemia likely plays a major role in trabecular bone loss. Importantly, cell autonomous activation of glycolysis in osteoblasts preserves both trabecular and cortical bone mass in the face of T1D. Thus, both hypoinsulinemia and hyperglycemia impinges on glycolysis in osteoblasts as an underlying cause for osteopenia in T1D.

The effect of insulin on glucose metabolism in bone has been a matter of debate. Although an early study detected stimulation of glucose uptake by insulin in rat calvarial bone sections, more recent work in the mouse reported no such effect in either calvarial osteoblast cultures or the long bones in vivo [26,27]. Yet another recent study by in vivo PET/CT imaging showed that insulin administration increased $^{18}$F-FDG uptake in murine bones [28]. Here by employing stable isotope tracing in vivo, we show clear stimulation of glycolysis by insulin in the cortical bone of both normal and diabetic mice. In keeping with the results in vivo, in vitro measurements with Seahorse extracellular flux analyzers confirm that

insulin stimulates glycolysis and oxidative phosphorylation in several different preparations of primary osteoblast-lineage cells. The observation that endosteal cells did not respond to insulin in the Seahorse assays could be significant as it might explain the lack of a trabecular bone phenotype following IR deletion. The lack of a trabecular bone response is also consistent with a recent study in T1D nonobese diabetic (NOD) mice that insulin therapy failed to improve trabecular bone mass or bone formation activity even though it restored periosteal bone formation [29]. Even so, the current study does not formally exclude loss of direct insulin signaling from contributing to the trabecular bone loss in T1D. Similar to T1D patients as previously reported, the Akita mice here also exhibit a slight reduction of circulating Igf1 (Supplemental Figure S1A)[30]. Therefore, loss of insulin, when combined with reduced Igf1 signaling, could potentially diminish trabecular bone accrual in T1D.

We show that overexpression of Glut1 accelerates diabetic bone loss. Although the underlying mechanism is not clear at present, the finding points to the detrimental effect of excessive glucose uptake by osteoblasts in diabetes. Hyperglycemia is known to cause multiple pathogenic changes in cells, as accumulation of intracellular glucose increases polyol pathway flux, protein modification through the hexosamine pathway and overproduction of mitochondrial superoxide [31]. It is conceivable that forced overexpression of Glut1 in our transgenic model further increases the intracellular glucose pool which in turn exacerbates the pathogenic pathways already active in diabetes, thus further impeding bone formation. Future studies are needed to determine whether increased polyol or hexosamine pathway or mitochondrial superoxide production plays a major role in diabetic osteopenia, and how they may contribute to the overall suppression of glycolysis in osteoblasts in response to hyperglycemia. Nonetheless, our data provide functional evidence that Glut1 downregulation in response to diabetes likely represents a protective mechanism for osteoblasts to restrict glucose uptake and to mitigate the associated detrimental effects.

It is worth noting that Pfkfb3 overexpression was less effective in countering bone loss in the older Akita mice. The reason for this is unclear at present, but it is possible that prolonged diabetes impairs downstream steps in the glycolysis pathway that cannot be restored by Pfkfb3 overexpression. For example, persistent activation of the polyol pathway which converts $NAD^+$ to NADH could diminish the $NAD^+$ pool that is necessary for sustaining glycolysis. In addition, activation of the polyol pathway reduces NADPH levels and therefore may disrupt glutathione homeostasis and de novo synthesis of fatty acids and nucleotides in osteoblasts. To address those possibilities, future experiments are necessary to determine whether simultaneous inhibition of the polyol pathway besides Pfkfb3 overexpression can restore bone mass in Akita mice with advanced diabetes.

Several previous studies have explored the role of glucose uptake and insulin signaling in normal bone formation. Transgenic expression of Glut1 via the Col1a1 promoter was reported to increase bone mass in the vertebrae of 3-month-old mice, but the study did not examine long bones [26]. In our study, overexpression of either Glut1 or Pfkfb3 did not cause a basal bone phenotype in long bones at either 8 or 20 weeks of age. It is not clear at present whether the apparent discrepancy reflects differences between the bones or the genetic tools. Regarding insulin signaling, others have reported that deletion of IR with osteocalcin-Cre (OC-Cre) resulted in loss of trabecular bone at 3 or 6 weeks of age without

affecting the cortical bone [10]. Here we show that deletion of IR by Prx1-Cre suppresses only cortical bone growth with no effect on trabecular bone at either 8 or 20 weeks of age. The lack of a cortical bone defect in the previous study could be due to OC-Cre targeting mainly mature osteoblasts without affecting the precursor cells. The discrepancy regarding the trabecular bone is less straightforward to reconcile but may reflect differences in the genetic background (C57BL/6 background here, unspecified in previous study) or the age of mice being analyzed. Alternatively, deletion of IR with Prx1-Cre in the mesenchymal progenitors may cause compensatory responses that do not occur with deletion in mature osteoblasts.

In summary, the current study supports the model that both hypoinsulinemia and hyperglycemia converge on glucose metabolism in osteoblasts to impair bone mass accrual in T1D. Similarly, we have recently shown that impaired osteoblast glycolysis drives bone loss in a mouse model for youth-onset type II diabetes[32]. Together, the findings provide a proof of principle that osteoblast glycolysis may be activated therapeutically to promote bone anabolism in diabetes.

### Limitations of the study

In the genetic rescue experiment, Pfkfb3 overexpression was activated at one week prior to the onset of T1D in the mouse. Future experiments are necessary to determine whether activation of glycolysis after the onset of T1D is sufficient to alleviate bone loss. The current study identifies impaired glycolysis as a major driver for bone loss during early T1D, but disruption of lipid metabolism, especially in advanced T1D, likely also contributes to diabetic bone loss. Future studies are warranted to delineate the disturbances of lipid metabolism, their relations to bone glucose metabolism and their role in diabetic osteopenia.

### Significance

Bone fragility is increasingly recognized as a comorbidity in diabetic patients. Type I diabetes especially is associated with decreased bone mineral density and a notable increase in fracture risks. Currently the two main classes of bone anabolic therapies are inadequate for diabetic patients due to contraindications of either cardiovascular complications or pediatric patients with open epiphysis. By investigating a monogenic type I diabetes mouse model, the present study discovers defective glycolysis in osteoblasts as an underlying cause for diabetic osteopenia. Furthermore, osteoblast-intrinsic activation of glycolysis is sufficient to preserve bone mass in the diabetic mouse. The results provide a proof of principle that osteoblast glycolysis may be therapeutically activated to minimize bone loss in diabetes.

## STAR Methods

### RESOURCE AVAILABILITY

**Lead contact—**Further information and requests for resources and reagents should be directed to and will be fulfilled by the lead contact, Fanxin Long (longf1@chop.edu).

**Materials availability—**The new mouse strain R26-TRE-Pfkfb3 is available upon execution of MTA.

### Data and code availability

- Single-cell and bulk RNA-seq data have been deposited at GEO and are publicly available as of the date of publication. The accession number is GSE232738.
- This paper does not report original code.
- Any additional information required to reanalyze the data reported in this paper is available from the lead contact upon request.

## EXPERIMENTAL MODEL AND STUDY PARTICIPANT DETAILS

**Mouse strains—**All mouse work was approved by the Children's Hospital of Philadelphia Animal Care and Use Committee. Mice were housed at 23°C with 12-h light circle with free access to food and water. Akita (#003548), Prx1-Cre (#005584), $IR^{f/f}$ (#006955), Ager-$CreER^{T2}$ (#36942) mouse strains were purchased from the Jackson Laboratory (Bar Harbor, ME). Osx-rtTA and Glut1-TRE mice are as previously described [33,34]. To create the R26-TRE-Pfkfb3 (herein TRE-Pfkfb3) mouse strain, a gene cassette consisting sequentially of CAG promoter, loxP-STOP-TRE-LoxP, Pfkfb3 CDS isoform 6 (NCBI NM 133232.3), P2A-eGFP and the bovine growth hormone gene (bGH) polyadenylation sequence was targeted into the Rosa26 locus in ES cells by homologous recombination. The correctly targeted ES cells were injected into blastocysts to create chimeric mice which were then mated with C57BL6/N to confirm germ-line transmission. Doxycycline food (TD.04104, ENVIGO) was used for activation of gene expression. Only male mice were studied as only male Akita mice developed severe T1D. Mice were studied mainly at 8 and 20 weeks of age but additional ages were used for several studies as indicated in figures and legends.

**Primary cell culture—**Primary cells were isolated from male and female mice without distinction. Primary calvarial cells were isolated and cultures according to a previous protocol [25]. Briefly, calvaria were dissected from murine neonates (P1-P5) and sequentially digested with collagenase I (Sigma, C0130) for multiple rounds of 15 mins at 37°C with gentle shaking. The cells were collected from the second through the fourth digestion. Isolation of periosteal cells was modified from a previous protocol [35]. In brief, tibias and femurs were dissected in HBSS buffer by removing the muscle and connective tissues with sharp scissors. Both ends of the bones were embedded in 3% (wt/vol) agarose (Lonza, 50101) before the bones were digested with 4 mg/ml dispase II (Roche, 04942078 001) and 3 mg/ml collagenase II (Worthington, LS004176) in MEM-α media at 37 °C in a shaker (Thermo Scintific MAXQ4450). Cells from the first 15-min digestion were discarded, and periosteal cells (PCs) were collected by combining the subsequent three 15-min digestions. PCs were passed through 70 μm-cell strainers and centrifuged at 500 rpm for 5 mins before being washed once and seeded into T25 flasks (Greiner, 690160) with complete MEM-α media containing 10% FBS (Thermo, 26140087) and Penicillin-Streptomycin (Thermo, 15140-122). PCs from one mouse (two tibias and two femurs) seeded into one flask normally reached confluency after 7 days.

For bone marrow stromal cells (BMSC), after the digestions for PCs, the epiphyses were removed with scissors from the bones. A 20-gauge needle connected with a syringe filled with MEM-α media containing 1% FBS was inserted from one end of the bone and then the

other to flush out the marrow until the diaphysis appeared white. The cells were centrifuged and resuspended in MEM-α media containing 10% FBS. After 7 days of culture with media changed on day 4, the cells were counted and depleted of hematopoietic cells with the MACS method according to manufacturer's instructions. Briefly, the cells were mixed with CD45 microbeads (Miltenyi Biotec, 130-052-301), washed, centrifuged and resuspended before being passed though LD columns (Miltenyi Biotec, 130-042-901) on a MidiMACS™ separator (Miltenyi Biotec, 130-042-302) attached to a multistand. The collected cells were seeded onto 10 cm cell culture plates at a seeding density of 500,000 cells per plate. For osteoblast differentiation, the purified BMSC were seeded at 30,000 cells/$cm^2$ in 12 well plate with MEMα containing 10% FBS, 4 mM β-glycerol phosphate (Sigma, G9422) and 50 ug/ml ascorbic acid (Sigma, A4544) with daily change of media for 10 days.

Endosteal cells were isolated from the trabecular bone and the bone shaft by enzymic digestion, after flushing of the bone marrow. After collection of BMSC, the remaining bone (containing metaphysis and diaphysis) was cut into small pieces and digested with 1 mg/ml dispase II (ThermoFisher Scientific, 17105041) and 1 mg/ml collagenase II (Worthington, LS004106) in 15 ml tubes for 30 mins. The cells were collected by centrifugation at 300 rpm for 5 min, washed with media and seeded in 10 cm cell culture plates at $5x10^6$ cells per plate. After 14 days of culture with media changes every 5 days, the $CD45^-$ cells were selected using the MACS method as for the BMSC.

Bone-chip cells were isolated from the bone chips after digestion of the endosteal cells. Briefly, the remaining bone chips were washed and incubated in the media for the cells to migrate out to the culture dishes under regular cell culture conditions for 14 days with media changes every 7 days. The $CD45^-$ cells were selected by using the MACS method.

## METHOD DETAILS

**In vitro metabolic assays—**Glucose consumption and lactate production rates by bone-chip cells were measured with a glucose (Sigma, GAHK20) or L-lactate assay kit (Eton Bioscience, 120001) after culturing the cells in a custom-made media (MEMα) based on ThermoFisher A10490, freshly supplemented with 5.5 mM glucose, 2 mM glutamine and 1 mM pyruvate for 24 hrs. The cells were seeded at 30,000 cells/$cm^2$ in 12-well plate.

For Seahorse assays, the seahorse plates were coated with PDL (Sigma, P7280) prior to use. PCs, BMSC, endosteal cells and bone chips cells were seeded in complete MEM-α at 40,000, 30,000, 30,000, and 20,000 cells per well, respectively, unless otherwise indicated in the figure legend. The seahorse assay medium (Agilent, 103575-100) was supplemented with 5.5 mM glucose, 2 mM glutamine and 1 mM pyruvate immediately before use. Six hours after seeding, the cells were switched to the seahorse assay medium for incubation in a non-$CO_2$ incubator at 37 °C for 1h, immediately before being assayed by Seahorse XFe96 Analyzer. In certain experiments, insulin was added to the seahorse assay media for the 1 hr incubation. Mitochondria stress test was performed by sequential injections of 4 μM oligomycin, 2 μM FCCP, 1 μM Rotenone and 1 μM Antimycin A (Agilent, 103010-100). Only commercial chemicals were used in the study.

**In vivo glucose tracing—**40 mg [$^{13}C_6$]Glc (Sigma, 389374) dissolved in PBS at 3.3 M concentration was injected via the tail vein at 40 mg/mouse after 5 hrs of fasting. At one hour after glc injection, the mice were sacrificed by cervical dislocation. The tibias and femurs were quickly dissected with the cartilage at both ends excised and the bone marrow removed by centrifugation for 1 min in each direction. The remaining mid-shafts were frozen with a pre-cooled Wollenberger clamp (Wollenberger et al., 1960) in liquid nitrogen. The bone mid-shafts were homogenized in 600 ul 4% perchloric acid (PCA) in water using Precellys homogenizer. After homogenization, the samples were centrifuged at 4°C and 2300g for 5 min, and the supernatants were to be used for metabolite quantification as previously described [25]. When insulin was tested, it was injected i.p. into WT mice immediately following [$^{13}$ $C_6$]glc injection, or into Akita mice 1 hr before [$^{13}$ $C_6$]glc injection. Glucose concentration was measured in plasma at different time points after insulin injection.

**Transcriptional activation with dCas9-SAM—**The dCas9-SAM method is as previously described [36]. Briefly, sgRNA was designed for specific genes (http://sam.genome-engineering.org/) and inserted into sgRNA (MS2) backbone (Addgene, 73797) by performing a golden gate assembly reaction (New England BioLabs, E2611L) (Supplemental Table VI). The Stbl3 strain cells (Thermo Fisher Scientific, C737303) were used form transformation. Correct insertion of sgRNA was verified by sequencing with the U6-fwd primer. To produce lentiviruses, 293T cells were transfected with pMD2.G, psPAX and the gene-specific target plasmid (sgPfkfb3, sgHk2 or sgLdha) at 70-80% confluency by using lipofectamine 2000 (Thermo Fisher Scientific, 11668019) and plus reagent (Thermo Fisher Scientific, 11514015). The primary calvarial cells were incubated with lentivirus-containing media for 8 hours before changing to regular complete media. At 72 hours after lentiviral infections, the cells were assayed for glucose consumption and lactate production, and harvested for western blotting.

**Serum CTX-I and P1NP assays—**Sera were collected by retro-orbital bleeding from mice after 6 hours of fasting. CTX-I and P1NP assays were performed, respectively, with the RatLaps ELISA and Rat/Mouse P1NP EIA Kit (Immunodiagnostic Systems, Ltd.).

**Histomorphometry and microCT analyses—**Paraffin sections were prepared according to routine procedures. TRAP staining was performed on paraffin sections following the standard protocol. For double labeling, the mice were injected with calcine (Sigma, C0875) at day 7 and alizarin red (Sigma, A3882) at day 2 before sacrifice. The bones were fixed in 4% PFA for 48 hours at room temperature, then transferred into 30% sucrose for 48 hours. The samples were cut at 10 μm and collected adherent to the cryofilm type IIC (10) (Section-Lab, Japan, CFS 105). The sections were scanned with AXIO (ZEISS, AXIO scan Z1) and quantified for bone formation parameters with BIOQUANT OSTEO 2021 V21.5.60.

For μCT, the femurs were scanned at 4.5 μm isotropic voxel size according to the guidelines of American Society of Bone and Mineral Research using MicroCT analysis (microCT45, Scanco Medical AG, Switzerland). For quantifying trabecular bone parameters, 500 CT slices (2.25mm total) immediately proximal to the distal femoral growth plate were analyzed

using a lower threshold of 350 and a Gaussian noise filter (sigma = 1.2, support = 2.0). For quantifying cortical bone parameter, 70 slices were analyzed using a lower threshold of 330 and a Gaussian noise filter (sigma = 1.2, support = 2.0).

**Western blot analyses—**The mid-shaft of femurs free of bone marrow by centrifugation was weighted and homogenized in M-PER extraction reagent (cat#78501, Thermo Scientific, Waltham, MA, USA) with a Precellys Evolution homogenizer (Bertin, Montigny-le-Bretonneux, France) at 6000 rpm for 15 seconds at 4 °C with 3 cycles. The supernatant was collected and centrifuged at 13000x g for 15 minutes. The protein concentration was determined by the BCA method (Thermo scientific, 23235) before electrophoresis in Nupage 4-12% Bis-Tris gel (Invitrogen, NP0322BOX) and transfer to the membrane (Sigma, IPFL00010) in the transfer buffer (Life technologies, NP0006-1). The membrane was incubated with a blocking buffer (Licor,927-60001) before with the specific primary antibodies against Glut1(abcam, ab1157730), Pfkfb3(abcam, ab181861), Ldha (Cell Signaling Technology, 2012), Hk2 (Abcam, ab228819), β-actin (Cell Signaling Technology, 3700). The membrane was finally incubated with a secondary anti-rabbit antibody (cat#926-32211, LICOR, Nebraska, USA) or anti-mouse antibody (cat#926-68070, LI-COR). Images were captured and quantified with the LI-COR software (LI-COR, Nebraska, USA).

**Bone RNA isolation, RT-qPCR and RNA-seq—**The bone diaphysis was cleanly dissected and immediately frozen in the liquid nitrogen in grinding tubes (Precellys, P000922-LYK0-A). The samples were homogenized (6000 rpm, 3x 10 sec) in 1 ml TRIzol (Ambion, 15596018) in a Precellys Evolution Homogenizer (Bertin Instruments). The homogenized samples were mixed with 1 mL RLT buffer with 2-mercaptoethanol and 2mL 70% ethanol, and then extracted for RNA according to the RNeasy mini kit protocol (Qiagen, #74106). Reverse transcription was conducted with High-Capacity RNA-to-cDNA kit (Thermo Scientific, 4387406), followed by qPCR with gene-specific primers and SYBR green mix (Applied Biosystems, 25742) in a Quantstudio3 machine (ABI) (Supplemental Table VII).

For RNA-seq, library construction, high-throughput sequencing and bioinformatics were performed by GENEWIZ, LLC./Azenta US, Inc (South Plainfield, NJ, USA). Extracted RNA samples were quantified using Qubit 2.0 Fluorometer (Life Technologies, Carlsbad, CA, USA) and RNA integrity was checked using Agilent TapeStation 4200 (Agilent Technologies, Palo Alto, CA, USA). RNA sequencing libraries were prepared using the NEBNext Ultra II RNA Library Prep Kit for Illumina following manufacturer's instructions (NEB, Ipswich, MA, USA). Briefly, mRNAs were first enriched with Oligo(dT) beads. Enriched mRNAs were fragmented for 15 minutes at 94 °C. First strand and second strand cDNAs were subsequently synthesized. cDNA fragments were end repaired and adenylated at 3'ends, and universal adapters were ligated to cDNA fragments, followed by index addition and library enrichment by limited-cycle PCR. The sequencing libraries were validated on the Agilent TapeStation (Agilent Technologies, Palo Alto, CA, USA), and quantified by using Qubit 2.0 Fluorometer (Invitrogen, Carlsbad, CA) as well as by quantitative PCR (KAPA Biosystems, Wilmington, MA, USA). The sequencing libraries

were clustered on 1 flowcell lane. After clustering, the flowcell was loaded on the Illumina HiSeq instrument (4000 or equivalent) according to manufacturer's instructions. The samples were sequenced using a 2x150bp Paired End (PE) configuration. Image analysis and base calling were conducted by the HiSeq Control Software (HCS). Raw sequence data (.bcl files) generated from Illumina HiSeq was converted into fastq files and de-multiplexed using Illumina's bcl2fastq 2.17 software. One mismatch was allowed for index sequence identification.

**Single cell RNA-seq—**For scRNA-seq, endosteal cells were isolated by using a protocol modified from a previous publication [37]. Tibias and femurs from three mice per group were harvested with the epiphysis surgically removed. The central bone marrow was flushed out with media (M-199 with 10% FBS and 1% P/S) and discarded, followed by scraping clean the periosteum with a scalpel. The metaphysis and mid-shafts were cut into small pieces with scissor. Bone pieces were digested with the STEMxyme1 (1 mg/ml, Worthington, LS004106) and Dispase II (1 mg/ml, ThermoFisher Scientific, 17105041) for 25 minutes at 37 °C in a cell culture shaker (ThermoFisher Scientific, MAXQ 4450). The digested cells were centrifuged at 300g for 3 mins and then suspended in 200 ul staining buffer (HBSS+2%FBS). Samples were stained in media 199 containing 2% FBS with the following reagents: CD45-PE (Invitrogen, 12-0451-82), CD3-PE (Biolegend, 100205), CD45R/B220-PE (Biolegend, 103207), CD19-PE (Biolegend, 115507), Gr1-PE (Biolegend, 108407), CD11b-PE (Biolegend, 101207), Ter119-APC (Invitrogen, 17-5921-82), CD71-PE/Cy7 (Biolegend, 113811), calcium AM (Invitrogen, C1430) and 7-AAD (Invitrogen, 00-6993). The cells were sorted with MoFlo Astrios Sorter (Beckman Coulter ) for the $7\text{-AAD}^{-}/\text{Calcein AM}^{+}/\text{CD71}^{-}/\text{Ter119}^{-}/\text{CD45}^{-}/\text{CD3}^{-}/\text{B220}^{-}/\text{CD19}^{-}\text{Gr-1}^{-}/\text{CD11b}^{-}$ fraction. The sorted single cells were counted and checked for cell viability with a hemocytometer, before they were used to construct barcoded scRNA-seq libraries by using the Chromium single cell 3' v2 reagent kit (CG000204_ChromiumNextGEMSingleCell3'v3.1, 10x Genomics). The cDNA libraries were sequenced on a NovaSeq 6000 SP Reagent Kit v1.5 (100 cycles) using sequencing run parameters 28x8x0x91.

Single-cell RNA-seq data were demultiplexed by processing with cell ranger, then aligned to mouse genome (mmlO). A total of 7829, 11161, 9920 or 12022 cells were sequenced for 8-week-old wild type, 8-week-old Akita, 20-week-old wild type or 20-week-old Akita, respectively. The medium number of genes detected per cell was 1607, 1486, 1119 or 1373 for those samples in the same order. The doublets and low-quality cells (genes > 6000, genes < 200, or >10% genes) were excluded. The feature expression for each cell was normalized by the total expression and multiplied by 10,000. The expression was log-transformed before subsequent analyses. The highly expressed feature gene was calculated using FindVariableFeatures() function [38]. A linear transformation ("scaling") was performed prior to dimension reduction. Principle component analysis (PCA) was performed on the scaled data and reduced the data to top 30 PCA components. The PCA-reduced data were then subjected to computing of a shared nearest neighbor graph, and were further subjected to graph-based clustering with the Louvain method. UMAP non-linear dimensional reduction was applied to the datasets to visualize the clusters. The differential expression of gene signatures was analyzed with wilcoxauc function. Based

on the gene signatures, the hematopoietic clusters were removed for sub-clustering of the mesenchymal cells, which was performed by repeating the same procedure of finding variable genes, dimensionality reduction, and clustering. For gene set enrichment analysis (GSEA), differential gene expression (wilcoxauc) between Akita and WT was used to generate a pre-ranked list for each cluster. Significantly affected pathways in each cluster between Akita and WT were determined by using Gene Set Enrichment Analysis (GSEA) with MsigDB gene sets [39].

### QUANTIFICATION AND STATISTICAL ANALYSIS

Statistics was performed with two-tailed unpaired Student's t-tests or two-way ANOVA followed by Fisher's LSD test. Details were provided in figure legends.

## Supplementary Material

Refer to Web version on PubMed Central for supplementary material.

## Acknowledgements

The work is supported by NIH grant R01 DK125498 (FL). We thank Penn Center for Musculoskeletal Disorders (PCMD) supported by NIH P30 AR069619 for service. We thank Haoran Liu for assistance with bioinformatics of scRNA-seq.

## References

1. Weber DR, Haynes K, Leonard MB, Willi SM, and Denburg MR (2015). Type 1 diabetes is associated with an increased risk of fracture across the life span: a population-based cohort study using The Health Improvement Network (THIN). Diabetes Care 38, 1913–1920. 10.2337/dc15-0783. [PubMed: 26216874]
2. Sellmeyer DE, Civitelli R, Hofbauer LC, Khosla S, Lecka-Czernik B, and Schwartz AV (2016). Skeletal Metabolism, Fracture Risk, and Fracture Outcomes in Type 1 and Type 2 Diabetes. Diabetes 65, 1757–1766. 10.2337/db16-0063. [PubMed: 27329951]
3. Ferrari SL, Abrahamsen B, Napoli N, Akesson K, Chandran M, Eastell R, El-Hajj Fuleihan G, Josse R, Kendler DL, Kraenzlin M, et al. (2018). Diagnosis and management of bone fragility in diabetes: an emerging challenge. Osteoporos Int 29, 2585–2596. 10.1007/s00198-018-4650-2. [PubMed: 30066131]
4. Janghorbani M, Feskanich D, Willett WC, and Hu F (2006). Prospective study of diabetes and risk of hip fracture: the Nurses' Health Study. Diabetes Care 29, 1573–1578. 10.2337/dc06-0440. [PubMed: 16801581]
5. Starup-Linde J, and Vestergaard P (2016). Biochemical bone turnover markers in diabetes mellitus - A systematic review. Bone 82, 69–78. 10.1016/j.bone.2015.02.019. [PubMed: 25722065]
6. Saag KG, Petersen J, Brandi ML, Karaplis AC, Lorentzon M, Thomas T, Maddox J, Fan M, Meisner PD, and Grauer A (2017). Romosozumab or Alendronate for Fracture Prevention in Women with Osteoporosis. N Engl J Med 377, 1417–1427. 10.1056/NEJMoa1708322. [PubMed: 28892457]
7. Lewiecki EM, Blicharski T, Goemaere S, Lippuner K, Meisner PD, Miller PD, Miyauchi A, Maddox J, Chen L, and Horlait S (2018). A Phase III Randomized Placebo-Controlled Trial to Evaluate Efficacy and Safety of Romosozumab in Men With Osteoporosis. J Clin Endocrinol Metab 103, 3183–3193. 10.1210/jc.2017-02163. [PubMed: 29931216]
8. Vahle JL, Sato M, Long GG, Young JK, Francis PC, Engelhardt JA, Westmore MS, Linda Y, and Nold JB (2002). Skeletal changes in rats given daily subcutaneous injections of recombinant human parathyroid hormone (1-34) for 2 years and relevance to human safety. Toxicol Pathol 30, 312–321. 10.1080/01926230252929882. [PubMed: 12051548]

9. Napoli N, Chandran M, Pierroz DD, Abrahamsen B, Schwartz AV, Ferrari SL, Bone IOF, and Diabetes Working G (2017). Mechanisms of diabetes mellitus-induced bone fragility. Nat Rev Endocrinol 13, 208–219. 10.1038/nrendo.2016.153. [PubMed: 27658727]
10. Fulzele K, Riddle RC, DiGirolamo DJ, Cao X, Wan C, Chen D, Faugere MC, Aja S, Hussain MA, Bruning JC, and Clemens TL (2010). Insulin receptor signaling in osteoblasts regulates postnatal bone acquisition and body composition. Cell 142, 309–319. 10.1016/j.cell.2010.06.002. [PubMed: 20655471]
11. Ferron M, Wei J, Yoshizawa T, Del Fattore A, DePinho RA, Teti A, Ducy P, and Karsenty G (2010). Insulin signaling in osteoblasts integrates bone remodeling and energy metabolism. Cell 142, 296–308. 10.1016/j.cell.2010.06.003. [PubMed: 20655470]
12. Irwin R, Lin HV, Motyl KJ, and McCabe LR (2006). Normal bone density obtained in the absence of insulin receptor expression in bone. Endocrinology 147, 5760–5767. 10.1210/en.2006-0700. [PubMed: 16973725]
13. Yamamoto M, and Sugimoto T (2016). Advanced Glycation End Products, Diabetes, and Bone Strength. Curr Osteoporos Rep 14, 320–326. 10.1007/s11914-016-0332-1. [PubMed: 27704396]
14. Esen E, Chen J, Karner CM, Okunade AL, Patterson BW, and Long F (2013). WNT-LRP5 signaling induces Warburg effect through mTORC2 activation during osteoblast differentiation. Cell metabolism 17, 745–755. 10.1016/j.cmet.2013.03.017. [PubMed: 23623748]
15. Karner CM, Esen E, Okunade AL, Patterson BW, and Long F (2015). Increased glutamine catabolism mediates bone anabolism in response to WNT signaling. The Journal of clinical investigation 125, 551–562. 10.1172/JCI78470. [PubMed: 25562323]
16. Esen E, Lee SY, Wice BM, and Long F (2015). PTH Promotes Bone Anabolism by Stimulating Aerobic Glycolysis Via IGF Signaling. Journal of bone and mineral research : the official journal of the American Society for Bone and Mineral Research. 10.1002/jbmr.2556.
17. Frey JL, Li Z, Ellis JM, Zhang Q, Farber CR, Aja S, Wolfgang MJ, Clemens TL, and Riddle RC (2015). Wnt-Lrp5 signaling regulates fatty acid metabolism in the osteoblast. Molecular and cellular biology 35, 1979–1991. 10.1128/MCB.01343-14. [PubMed: 25802278]
18. Lee SY, and Long F (2018). Notch signaling suppresses glucose metabolism in mesenchymal progenitors to restrict osteoblast differentiation. J Clin Invest 128, 5573–5586. 10.1172/JCI96221. [PubMed: 30284985]
19. Wang J, Takeuchi T, Tanaka S, Kubo SK, Kayo T, Lu D, Takata K, Koizumi A, and Izumi T (1999). A mutation in the insulin 2 gene induces diabetes with severe pancreatic beta-cell dysfunction in the Mody mouse. J Clin Invest 103, 27–37. 10.1172/JCI4431. [PubMed: 9884331]
20. Yoshioka M, Kayo T, Ikeda T, and Koizumi A (1997). A novel locus, Mody4, distal to D7Mit189 on chromosome 7 determines early-onset NIDDM in nonobese C57BL/6 (Akita) mutant mice. Diabetes 46, 887–894. 10.2337/diab.46.5.887. [PubMed: 9133560]
21. Oyadomari S, Koizumi A, Takeda K, Gotoh T, Akira S, Araki E, and Mori M (2002). Targeted disruption of the Chop gene delays endoplasmic reticulum stress-mediated diabetes. J Clin Invest 109, 525–532. 10.1172/JCI14550. [PubMed: 11854325]
22. Coe LM, Zhang J, and McCabe LR (2013). Both spontaneous Ins2(+/−) and streptozotocin-induced type I diabetes cause bone loss in young mice. J Cell Physiol 228, 689–695. 10.1002/jcp.24177. [PubMed: 22886636]
23. Hu P, McKenzie JA, Buettmann EG, Migotsky N, Gardner MJ, and Silva MJ (2021). Type 1 diabetic Akita mice have low bone mass and impaired fracture healing. Bone 147, 115906. 10.1016/j.bone.2021.115906. [PubMed: 33662611]
24. Baccin C, Al-Sabah J, Velten L, Helbling PM, Grunschlager F, Hernandez-Malmierca P, Nombela-Arrieta C, Steinmetz LM, Trumpp A, and Haas S (2020). Combined single-cell and spatial transcriptomics reveal the molecular, cellular and spatial bone marrow niche organization. Nat Cell Biol 22, 38–48. 10.1038/s41556-019-0439-6. [PubMed: 31871321]
25. Lee WC, Ji X, Nissim I, and Long F (2020). Malic Enzyme Couples Mitochondria with Aerobic Glycolysis in Osteoblasts. Cell Rep 32, 108108. 10.1016/j.celrep.2020.108108. [PubMed: 32905773]
26. Wei J, Shimazu J, Makinistoglu MP, Maurizi A, Kajimura D, Zong H, Takarada T, Iezaki T, Pessin JE, Hinoi E, and Karsenty G (2015). Glucose Uptake and Runx2 Synergize to Orchestrate

Osteoblast Differentiation and Bone Formation. Cell 161, 1576–1591. 10.1016/j.cell.2015.05.029. [PubMed: 26091038]

27. Hahn TJ, Westbrook SL, Sullivan TL, Goodman WG, and Halstead LR (1988). Glucose transport in osteoblast-enriched bone explants: characterization and insulin regulation. J Bone Miner Res 3, 359–365. 10.1002/jbmr.5650030317. [PubMed: 2463740]
28. Zoch ML, Abou DS, Clemens TL, Thorek DL, and Riddle RC (2016). In vivo radiometric analysis of glucose uptake and distribution in mouse bone. Bone research 4, 16004. 10.1038/boneres.2016.4. [PubMed: 27088042]
29. Dixit M, Liu Z, Poudel SB, Yildirim G, Zhang YZ, Mehta S, Murik O, Altarescu G, Kobayashi Y, Shimizu E, et al. (2021). Skeletal Response to Insulin in the Naturally Occurring Type 1 Diabetes Mellitus Mouse Model. JBMR Plus 5, e10483. 10.1002/jbm4.10483. [PubMed: 33977201]
30. Teppala S, and Shankar A (2010). Association between serum IGF-1 and diabetes among U.S. adults. Diabetes Care 33, 2257–2259. 10.2337/dc10-0770. [PubMed: 20639451]
31. Shah MS, and Brownlee M (2016). Molecular and Cellular Mechanisms of Cardiovascular Disorders in Diabetes. Circ Res 118, 1808–1829. 10.1161/CIRCRESAHA.116.306923. [PubMed: 27230643]
32. Song F, Lee WD, Marmo T, Ji X, Song C, Liao X, Seeley R, Yao L, Liu H, and Long F (2023). Osteoblast-intrinsic defect in glucose metabolism impairs bone formation in type II diabetic male mice. Elife 12. 10.7554/eLife.85714.
33. Song D, He G, Song F, Wang Z, Liu X, Liao L, Ni J, Silva MJ, and Long F (2020). Inducible expression of Wnt7b promotes bone formation in aged mice and enhances fracture healing. Bone Res 8, 4. 10.1038/s41413-019-0081-8. [PubMed: 32047703]
34. Pereira RO, Wende AR, Olsen C, Soto J, Rawlings T, Zhu Y, Anderson SM, and Abel ED (2013). Inducible overexpression of GLUT1 prevents mitochondrial dysfunction and attenuates structural remodeling in pressure overload but does not prevent left ventricular dysfunction. J Am Heart Assoc 2, e000301. 10.1161/JAHA.113.000301. [PubMed: 24052497]
35. van Gastel N, Torrekens S, Roberts SJ, Moermans K, Schrooten J, Carmeliet P, Luttun A, Luyten FP, and Carmeliet G (2012). Engineering vascularized bone: osteogenic and proangiogenic potential of murine periosteal cells. Stem Cells 30, 2460–2471. 10.1002/stem.1210. [PubMed: 22911908]
36. Joung J, Konermann S, Gootenberg JS, Abudayyeh OO, Platt RJ, Brigham MD, Sanjana NE, and Zhang F (2017). Genome-scale CRISPR-Cas9 knockout and transcriptional activation screening. Nat Protoc 12, 828–863. 10.1038/nprot.2017.016. [PubMed: 28333914]
37. Baryawno N, Przybylski D, Kowalczyk MS, Kfoury Y, Severe N, Gustafsson K, Kokkaliaris KD, Mercier F, Tabaka M, Hofree M, et al. (2019). A Cellular Taxonomy of the Bone Marrow Stroma in Homeostasis and Leukemia. Cell 177, 1915–1932 e1916. 10.1016/j.cell.2019.04.040. [PubMed: 31130381]
38. Satija R, Farrell JA, Gennert D, Schier AF, and Regev A (2015). Spatial reconstruction of single-cell gene expression data. Nat Biotechnol 33, 495–502. 10.1038/nbt.3192. [PubMed: 25867923]
39. Subramanian A, Tamayo P, Mootha VK, Mukherjee S, Ebert BL, Gillette MA, Paulovich A, Pomeroy SL, Golub TR, Lander ES, and Mesirov JP (2005). Gene set enrichment analysis: a knowledge-based approach for interpreting genome-wide expression profiles. Proc Natl Acad Sci U S A 102, 15545–15550. 10.1073/pnas.0506580102. [PubMed: 16199517]

## Highlights

1. T1D impairs glycolysis in bone
2. Insulin stimulates, and hyperglycemia diminishes glucose metabolism in osteoblasts
3. Loss of insulin signaling reduces cortical but not trabecular bone accrual
4. Genetic activation of glycolysis preserves bone mass in T1D

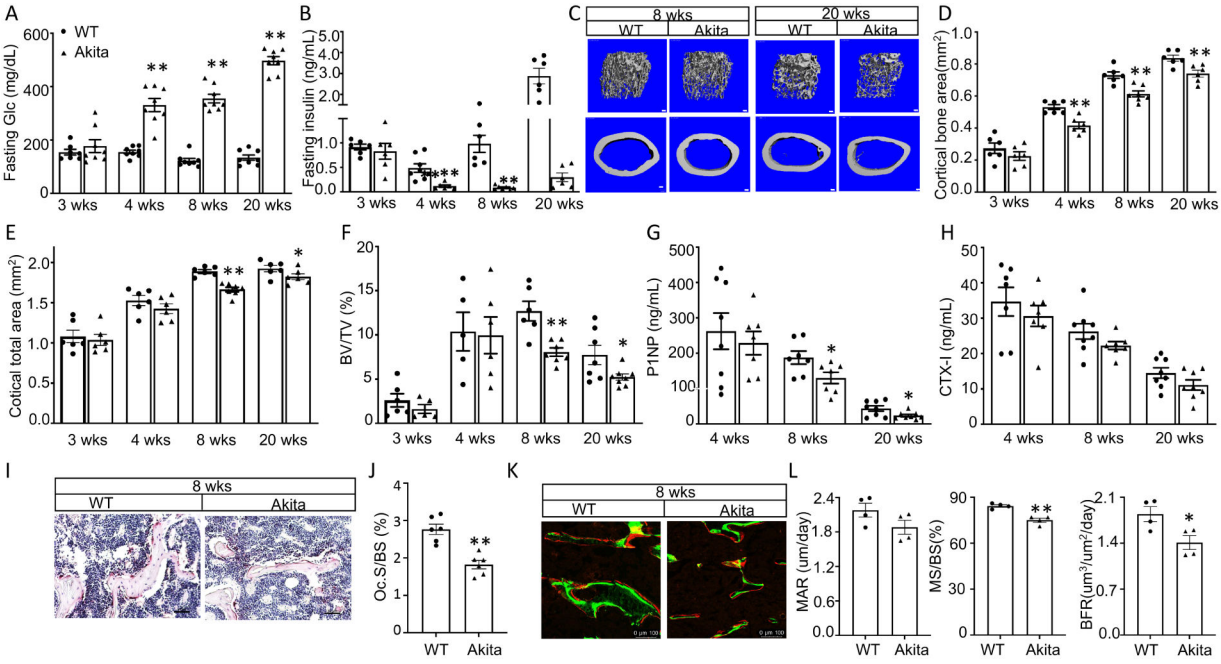


**Figure 1. Akita T1D mice exhibit osteopenia due to impaired bone formation.**

(A, B) Fasting glucose (A) or insulin (B) levels of male mice at different ages. (C) Representative images of trabecular (upper) and cortical (lower) bone following 3-D reconstruction of the femur by ***μ***CT. Scale bar: 100 μm. (D-F) Quantitation of cortical (D, E) and trabecular (F) bone parameters by ***μ***CT. (G, H) Serum P1NP (G) or CTX-I (H) levels. (I, J) Representative images (I) and quantification (J) of TRAP staining in trabecular bone region. TRAP signal in red. Scale bar: 50 μm. (K, L) Representative images (K) and quantification (L) of double labeling in trabecular bone region. Scale bar: 100 μm. Green label: calcein; red label: alizarin red. All bar graphs: circles and triangles denote individual wild type (WT) and Akita mice, respectively. * $p<0.05$, ** $p<0.01$, Student's t test. Error bars: SEM.

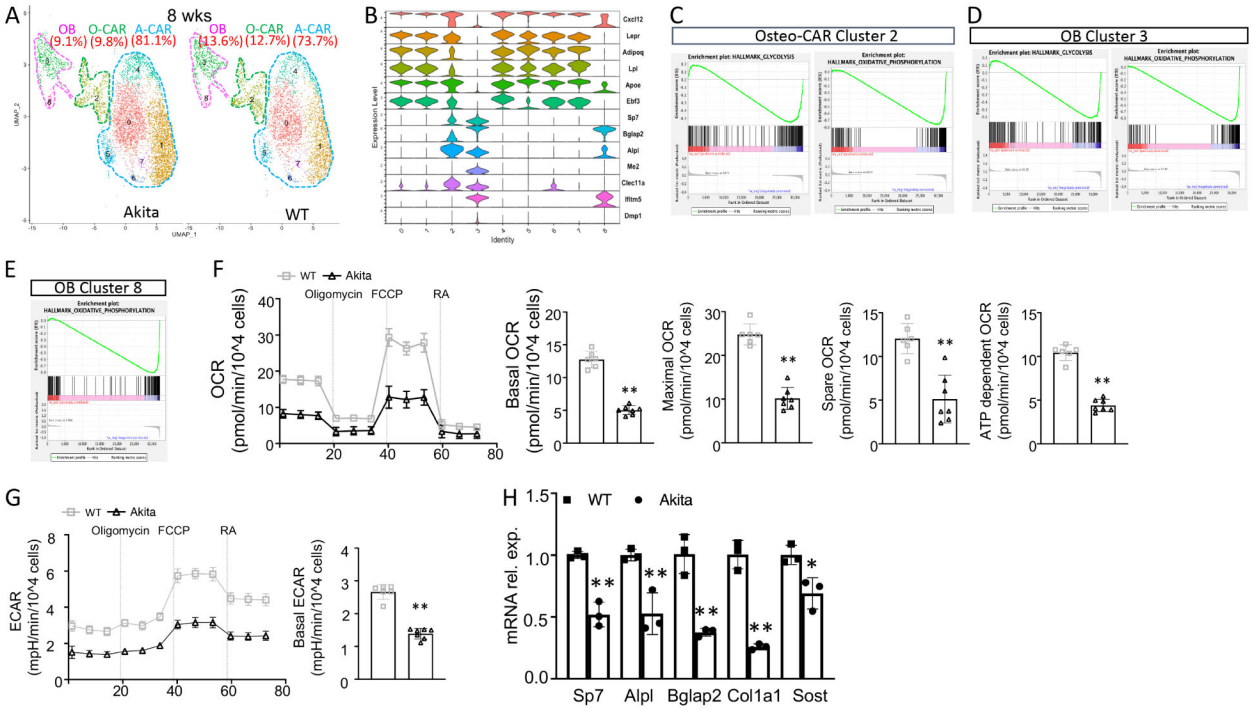


**Figure 2. T1D causes metabolic and osteogenic defects in osteoblast-lineage cells.**

(A) Identification of clusters among endosteal cells by scRNA-seq in 8-wk-old mice. OB: osteoblast; O-OAR: Osteo-CAR; A-CAR: Adipo-CAR. Percentages in parentheses denote relative abundance. (B) Violin plots of representative molecular markers used for cluster annotation. (C-E) GSEA graphs showing negative enrichment scores for glycolysis and OXPHOS in T1D vs WT osteogenic clusters. (F, G) Seahorse measurements of OCR (F) and ECAR (G) in endosteal cells from 8-wk-old WT (squares) vs Akita (triangles) mice. The cells were seeded at 35,000 cells per Seahorse well. Basal ECAR referred to value at last time point before oligomycin injection (3$^{rd}$ measurement). (H) RT-qPCR of osteoblast markers following in vitro differentiation of BMSC. * $p<0.05$, ** $p<0.01$, Student's t test. Error bars: SD.

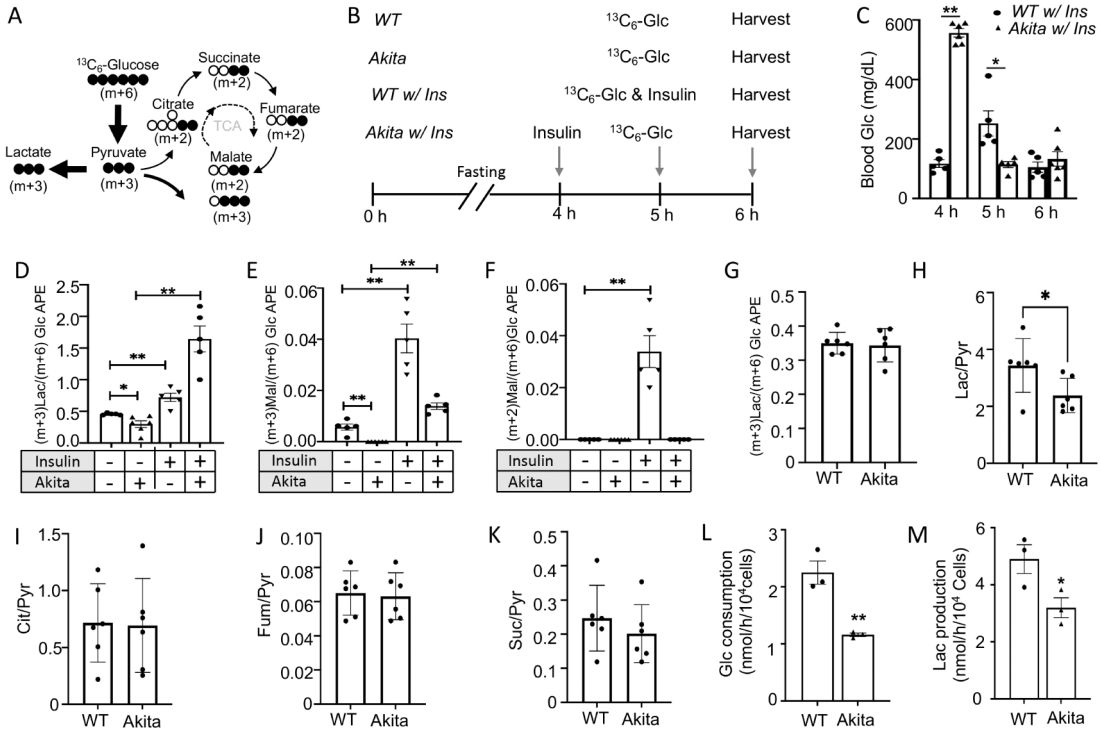


**Figure 3. Insulin stimulates and T1D impairs glycolysis in bone.**

(A) Diagram for glucose carbon contribution to glycolysis and TCA metabolite. Closed and open circles denote $^{13}C$ and $^{12}C$, respectively. Thickness of lines denotes relative flux based on previous findings in osteoblasts. (B) Schematic for glucose tracing. (C) Blood glucose levels during tracing in 20-week-old mice. (D-G) Enrichment of labeled metabolites relative to labeled glucose in bone at 20 (D-F) or 8 (G) weeks of age. (H-K) Abundance of metabolites normalized to pyruvate in bone. APE: atom percentage excess. (L, M) Measurements of glucose consumption (L) and lactate production (M) rate in bone-chip cells. * $p<0.05$, ** $p<0.01$, Student's t test. Error bars: SEM.

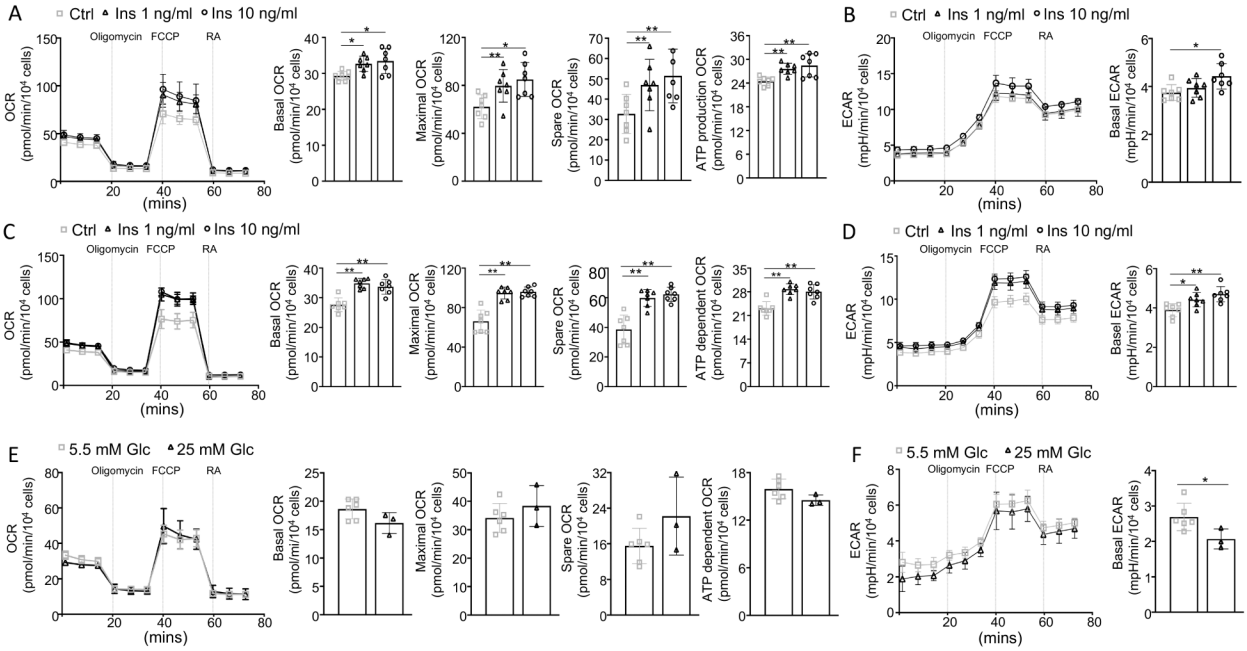


**Figure 4. Insulin stimulates and chronic hyperglycemia suppresses metabolism in osteoblast-lineage cells.**

(A-D) Seahorse assays of bone-chip cells (A, B) or BMSC (C, D) with or without insulin treatment for 1h. (E, F) Seahorse assays of bone-chip cells cultured with normal or high concentrations of glucose for 14 days. * $p<0.05$, ** $p<0.01$, Student' t test. Error bars: SD.

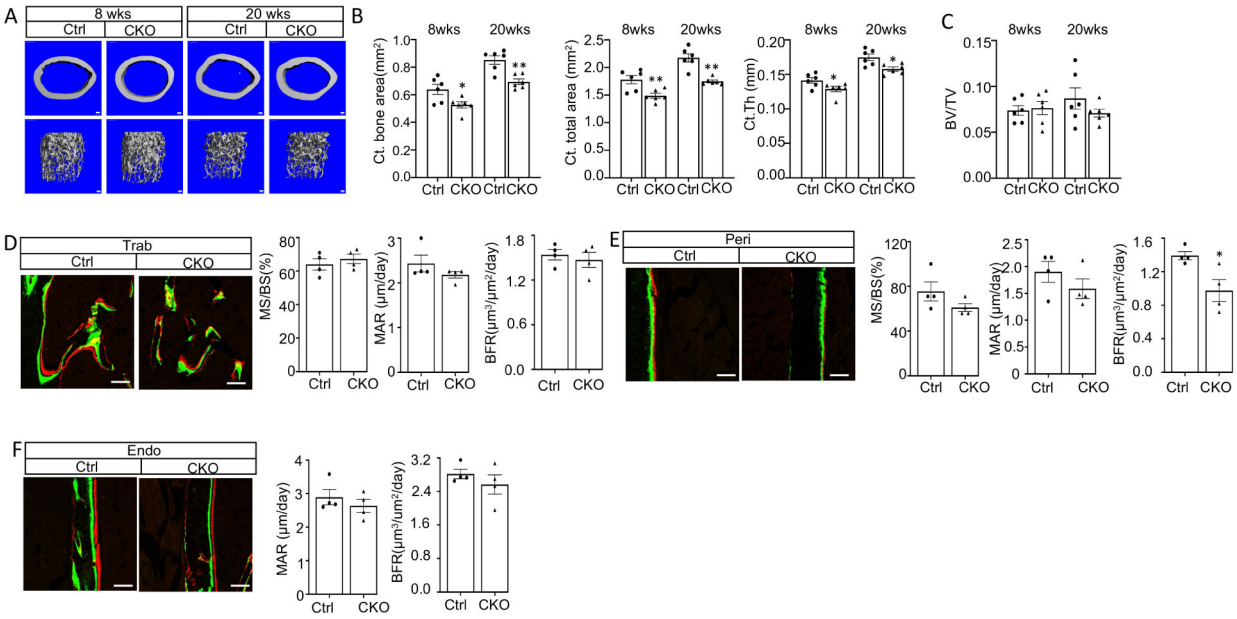


**Figure 5. Insulin signaling is required for periosteal but not trabecular bone accrual.**

(A) Representative images of cortical (upper) and trabecular (lower) bone following 3-D reconstruction by μCT. Ctrl: $IR^{f/f}$; CKO: Prx1-Cre;$IR^{f/f}$. Scale bar: 100 μm. (B, C) Quantification of cortical (B) and trabecular (C) bone parameters by μCT. (D-F) Representative images and quantification of double labeling in trabecular bone (D), at the periosteum (E) and endosteum (F). Scale bar: 100 μm. *p<0.05, **p<0.01, Student's t test. Error bars: SEM.

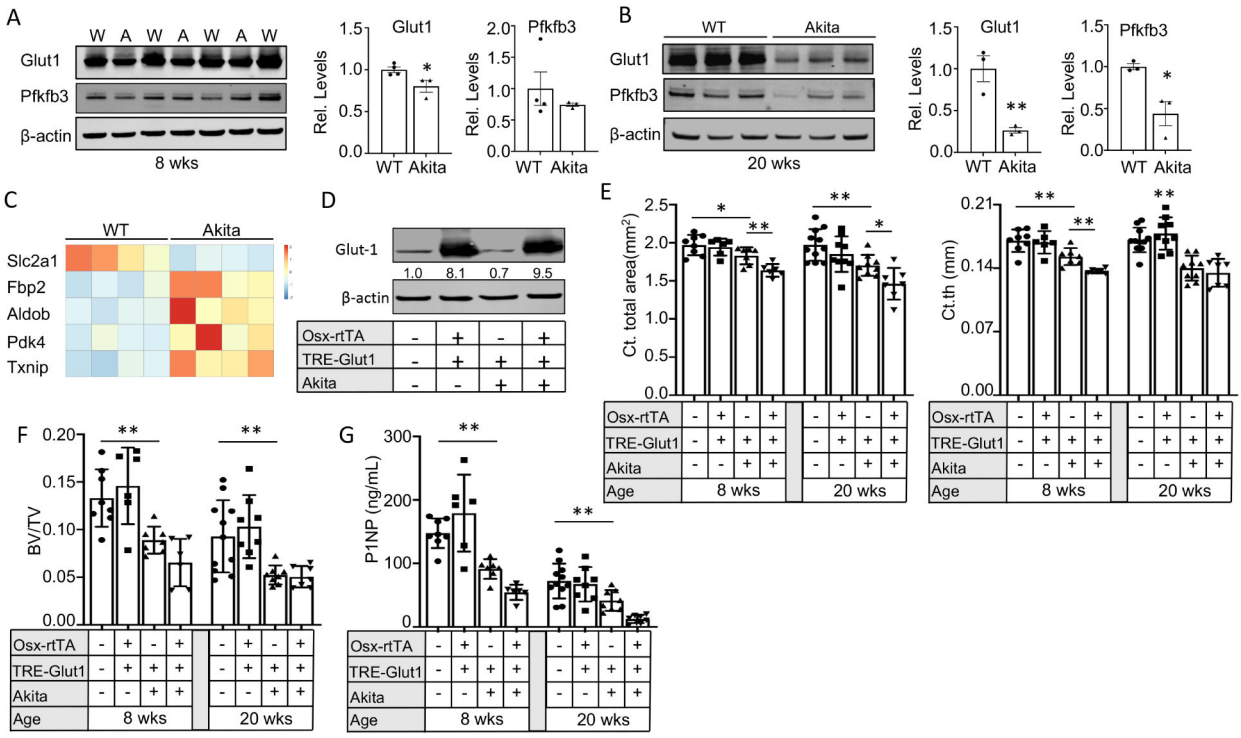


**Figure 6. Glut1 overexpression worsens bone loss in T1D.**

(A, B) Western blot images and quantification for cortical bone protein extracts at 8 (A) and 20 (B) weeks of age. W: Wild type; A: Akita. Relative Glut1 or Pfkfb3 levels calculated over wild type after normalization to ß-actin. (C) Heatmap from RNA-seq of cortical bone RNA at 20 weeks. Scale indicates $log_2$FC values. (D) Western blot with bone protein extracts from wild type (Akita−) or Akita mice (Akita+) with or without Glut1 overexpression (Osx-rtTA+, TRE-Glut1+) and harvested at 8 weeks of age. Glut1 intensity normalized to ß-actin as loading control. (E, F) Quantification of cortical (E) and trabecular (F) bone parameters by µCT. (G) Quantification of serum P1NP levels. *p<0.05, **p<0.01, Student's t test (A, B) or two-way ANOVA (E-G). Error bars: SEM.

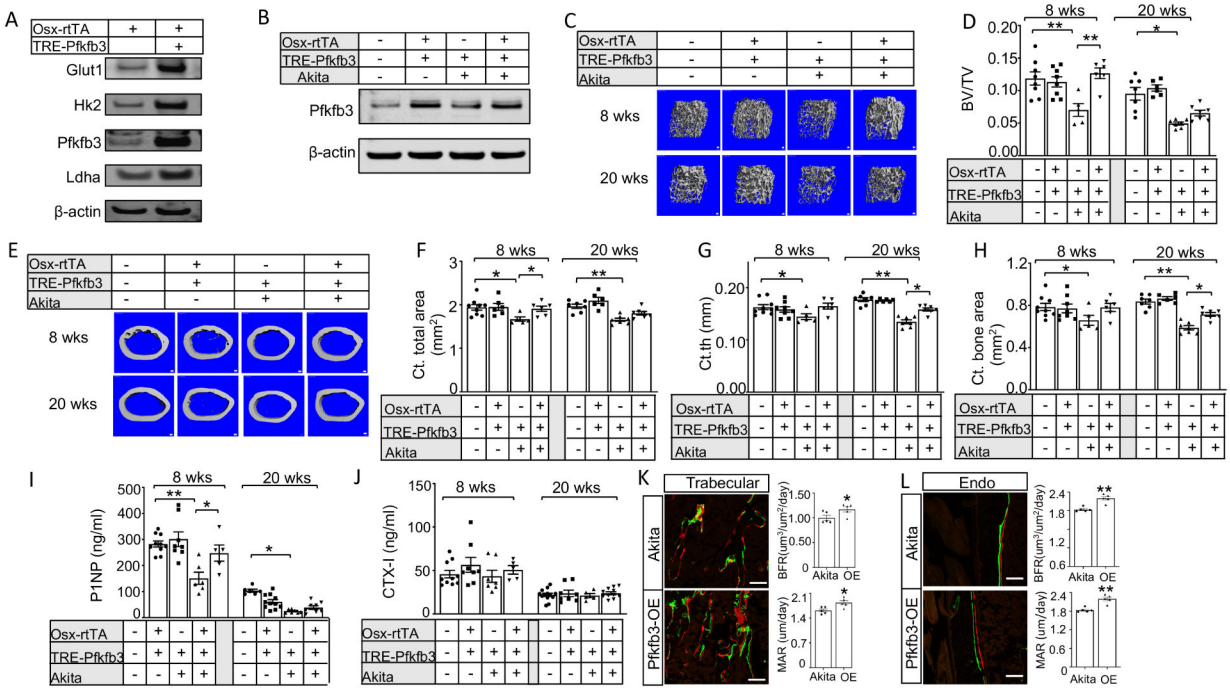


**Figure 7. Pfkfb3 overexpression prevents early bone loss in Akita mice.**

(A) Western blot of bone protein extracts from mice with indicated genotypes treated with Dox from 3 through 8 weeks of age. (B) Western blot of bone protein extracts from wild type (Akita−) or Akita mice (Akita+) with or without Glut1 overexpression (Osx-rtTA+, TRE-Pfkfb3+) treated with Dox from 3 through 8 weeks of age. (C, D) Representative ***μ***CT images (C) and quantification (D) of trabecular bone. (E-H) Representative ***μ***CT images (E) and quantification (F-H) of cortical bone parameters. (I, J) Serum P1NP (I) and CTX-I levels (J). (K, L) Representative images and quantification of double labeling in trabecular bone region (K) and at the endosteum of cortical bone (L). Scale bar: 100 μm. *p<0.05, **p<0.01, two-way ANOVA (D, F-J), Student's t test (I-L). Error bars: SEM.

Key resources table

| REAGENT or RESOURCE | SOURCE | IDENTIFIER |
|---|---|---|
| Antibodies | | |
| Rabbit monoclonal anti-Glut1 | Abcam | Cat#ab1157730 |
| Rabbit monoclonal anti-Pfkfb3 | Abcam | Cat#ab181861 |
| Rabbit polyclonal anti-Ldha | Cell Signaling Technology | Cat#2012 |
| Rabbit monoclonal anti-Hk2 | Abcam | Cat#ab228819 |
| Mouse monoclonal anti-β-actin | Cell Signaling Technology | Cat#3700 |
| CD45 | Invitrogen | Cat#12-0451-82 |
| CD3 | Biolegend | Cat#100205 |
| CD45R/B220 | Biolegend | Cat#103207 |
| CD19 | Biolegend | Cat#115507 |
| Gr1 | Biolegend | Cat#108407 |
| CD11b | Biolegend | Cat#101207 |
| Ter119 | Invitrogen | Cat#17-5921-82 |
| CD71 | Biolegend | Cat#113811 |
| Secondary anti-rabbit antibody | LICOR | Cat#926-32211 |
| Secondary anti-mouse antibody | LICOR | Cat#926-68070 |
| Chemicals, peptides, and recombinant proteins | | |
| Agarose | Lonza | Cat#50101 |
| Collagenase I | Sigma | Cat#C0130 |
| Dispase II (Periosteal cells) | Roche | Cat#04942078001 |
| Collagenase II | Worthington | Cat#LS004176 |
| FBS | Thermo Fisher Scientific | Cat#26140087 |
| CD45 microbeads | Miltenyi Biotec | Cat#130-052-301 |
| Ascorbic acid | Sigma | Cat#A4544 |
| β-glycerol phosphate | Sigma | Cat#G9422 |
| Dispase II (Endosteal cells) | Thermo Fisher Scientific | Cat#17105041 |
| Custom-made media (MEMα) | Thermo Fisher Scientific | Cat#A10490 |
| D-(+)-Glucose | Sigma | Cat#G7021 |
| L-Glutamine | Thermo Fisher Scientific | Cat#25030081 |
| Sodium pyruvate | Sigma | Cat#P5280 |
| Poly-D-Lysine | Sigma | Cat#P7280 |
| Seahorse assay medium | Agilent | Cat#103575-100 |
| Oligomycin | Sigma | Cat#O4876 |
| Rotenone | Sigma | Cat#R8875 |
| Antimycin A | Antimycin A | Cat#A8674 |
| Uniformly labeled $^{13}$C-D-glucose | Sigma | Cat#389374 |
| Calcine | Sigma | Cat#C0875 |

| REAGENT or RESOURCE | SOURCE | IDENTIFIER |
|---|---|---|
| Alizarin red | Sigma | Cat#A3882 |
| M-PER extraction reagent | Thermo Fisher Scientific | Cat#78501 |
| TRIzol | Ambion | Cat#15596018 |
| SYBR green mix | Applied Biosystems | Cat#25742 |
| 7-AAD | Invitrogen | Cat#00-6993 |
| Calcium AM | Invitrogen | Cat#C1430 |
| Plus reagent | Thermo Fisher Scientific | Cat#11514015 |
| lipofectamine 2000 | Thermo Fisher Scientific | Cat#11668019 |
| Critical commercial assays | | |
| Glucose (HK) Assay Kit | Sigma | Cat#GAHK20 |
| L-Lactate Assay Kit I | Eton Bioscience | Cat#120001 |
| Rat/Mouse P1NP EIA Kit | Immunodiagnostic Systems, Ltd. | Cat#AC-33F1 |
| RatLaps ELISA | Immunodiagnostic Systems, Ltd. | Cat#AC-06F1 |
| RNeasy mini kit | Qiagen | Cat#74106 |
| High Capacity RNA-to-cDNA kit | Thermo Scientific | Cat#4387406 |
| BCA kit | Thermo scientific | Cat#23235 |
| Deposited data | | |
| Raw and analyzed data | This paper | GEO: GSE232738 |
| Experimental models: Organisms/strains | | |
| Mouse: Akita | The Jackson Laboratory | JAX:003548 |
| Mouse: Prx1-Cre | The Jackson Laboratory | JAX:005584 |
| Mouse: $IR^{f/f}$ | The Jackson Laboratory | JAX:006955 |
| Mouse: Osx-rtTA | Dr. Fanxin Long | Ref. 33 |
| Mouse: Glut1-TRE | Dr. E. Dale Abel | Ref. 34 |
| Mouse: TRE-Pfkfb3 | This paper | N/A |
| Oligonucleotides | | |
| Primers for RT-qPCR, see Table S VI | This paper | N/A |
| Primers for sgRNA, see Table S VII | This paper | N/A |
| Recombinant DNA | | |
| Lenti sgRNA(MS2)_puro | Addgene | Cat#73797 |
| pMD2.G | Addgene | Cat#12259 |
| psPAX2 | Addgene | Cat#12260 |
| Software and algorithms | | |
| Cell Ranger | 10X Genomics | https://support.10xgenomics.com/single-cell-gene-expression/software/overview/welcome |
| Seurat (version 4.1.0) | Stuart et al. 2019 | https://satijalab.org/seurat/ |
| R (version 4.0.3) | R core team, 2020 | https://www.r-project.org/ |
| GSEA | Subramanian et al. 2005 Mootha et al. 2003 | https://www.gsea-msigdb.org/gsea/index.jsp |